

# Neutron star properties in density dependent relativistic Hartree-Fock theory

Bao Yuan Sun,<sup>1</sup> Wen Hui Long,<sup>1,2</sup> Jie Meng,<sup>1,3,4,5</sup> and U. Lombardo<sup>6,7</sup>

<sup>1</sup>*School of Physics and State Key Laboratory of Nuclear Physics and Technology,  
Peking University, 100871 Beijing, China*

<sup>2</sup>*Physik-Department der Technischen Universität München, D-85748 Garching, Germany*

<sup>3</sup>*Department of Physics, University of Stellenbosch, Stellenbosch, South Africa*

<sup>4</sup>*Institute of Theoretical Physics, Chinese Academy of Sciences, 100080 Beijing, China*

<sup>5</sup>*Center of Theoretical Nuclear Physics, National Laboratory  
of Heavy Ion Accelerator, 730000 Lanzhou, China*

<sup>6</sup>*Laboratori Nazionali del Sud, Istituto Nazionale di Fisica Nucleare, Via S. Sofia 62, I-95123 Catania, Italy*

<sup>7</sup>*Dipartimento di Fisica e Astronomia, Università di Catania,  
viale Andrea Doria 6, I-95125 Catania, Italy*

With the equations of state provided by the newly developed density dependent relativistic Hartree-Fock (DDRHF) theory for hadronic matter, the properties of the static and  $\beta$ -equilibrium neutron stars without hyperons are studied for the first time, and compared to the predictions of the relativistic mean field (RMF) models and recent observational data. The influences of Fock terms on properties of asymmetric nuclear matter at high densities are discussed in details. Because of the significant contributions from the  $\sigma$ - and  $\omega$ -exchange terms to the symmetry energy, large proton fractions in neutron stars are predicted by the DDRHF calculations, which strongly affect the cooling process of the star. The critical mass about  $1.45 M_{\odot}$ , close to the limit  $1.5 M_{\odot}$  determined by the modern soft X-ray data analysis, is obtained by DDRHF with the effective interactions PKO2 and PKO3 for the occurrence of direct Urca process in neutron stars. The maximum masses of neutron stars given by the DDRHF calculations lie between  $2.45 M_{\odot}$  and  $2.49 M_{\odot}$ , which are in reasonable agreement with high pulsar mass  $2.08 \pm 0.19 M_{\odot}$  from PSR B1516+02B. It is also found that the mass-radius relations of neutron stars determined by DDRHF are consistent with the observational data from thermal radiation measurement in the isolated neutron star RX J1856, QPOs frequency limits in LMXBs 4U 0614+09 and 4U 1636-536, and redshift determined in LMXBs EXO 0748-676.

PACS numbers: 21.30.Fe, 21.60.Jz, 21.65.-f, 26.60.-c

## I. INTRODUCTION

The investigative territory of nuclear physics has been enormously expanded with the construction of the new accelerator facilities as well as the development of the land- and space-based observatories. The exploration over the phase diagram of matter has been extended to the extreme conditions of density, pressure and temperature during the last several decades, which is

now one of the hottest topics in both theoretical and experimental nuclear physics. While around the saturation density, the nuclear matter properties can be well calibrated by terrestrial experiments with the atomic nuclei, the neutron stars are the natural laboratories in the universe for exploring the equation of state (EoS) of baryonic matter at low temperature and higher baryonic densities [1, 2, 3]. In addition, the probe to the elliptical flow and kaon production in heavy-ion collisions provides extra information for the nuclear EoS at high temperature and about  $2 \sim 4.5$  times nuclear saturation density [4, 5, 6].

As one of the most exotic objects in the universe, neutron star plays the role of a bridge between nuclear physics and astrophysics. With the discovery of neutron in 1932, the concept of the neutron star were firstly proposed by Landau [7]. Two years later, the neutron star was deemed to be formed in *supernovae* [8]. In 1960s, the observed radio pulsars [9] were identified as the rotating neutron stars [10]. Currently the neutron star is generally considered to be of the crust structure [11]. Below the atmosphere and envelope surface with a negligible amount of mass, the crust extends about 1 to 2 km into star, which mainly consists of nuclei and free electrons. With the density increasing, the dominant nuclei in the crust vary from  $^{56}\text{Fe}$  to extremely neutron-rich nuclei and neutrons may gradually leak out of nuclei to form the neutron fluid. The outer core ( $\rho \gtrsim \rho_0/3$ ) of neutron stars is composed of a soup of nucleons, electrons, and muons. In the inner core, exotic particles may become abundant, such as the strangeness-bearing hyperons and/or Bose condensates (pions or kaons), and a transition to a mixed phase of hadronic and deconfined quark matter becomes possible. Although similar EoS at saturation and subsaturation densities is obtained by various nuclear matter models, their deviations are very remarkable in the high density region, which is very essential in describing and predicting the properties of neutron stars. Further investigations are therefore necessitated for the detailed structure over the density range of neutron stars.

The recent observations of neutron stars have been reviewed, such as in Ref. [12]. The existence of massive compact stars of  $2 M_\odot$  or above is now unveiled by some evidence. Careful analysis of the *Rossi X-ray Timing Explorer (RXTE)* data for the quasi-periodic brightness oscillations (QPOs) discovered from low-mass X-ray binaries (LMXBs) 4U 1636-536 shows that several neutron stars in LMXBs have the gravitational masses between  $1.9 M_\odot$  and possibly  $2.1 M_\odot$  [13]. Measurements on millisecond pulsars in globular cluster NGC 5904 (M5) during 19 years of Arecibo timing yield  $M = 2.08 \pm 0.19 M_\odot$  for PSR B1516+02B [14]. Whereas a much larger pulsars mass  $2.74 \pm 0.21 M_\odot$  is presented very recently for PSR J1748-2021B in NGC 6440 [15]. Besides the maximum mass limits, the mass-radius relation is also constrained by the recent observations. The thermal radiation spectra in X-rays and in optical-UV from the isolated neutron star RX J1856.5-3754 (shorthand: RX J1856) determine the large radiation radius  $R_\infty$  as 16.8 km [16]. The model fitting to the high-quality X-ray spectrum of the quiescent LMXB X7 in the globular cluster 47 Tuc prefers a

rather large radius of  $14.5_{-1.6}^{+1.8}$  km for a  $1.4 M_{\odot}$  compact star [17]. In another LMXB, EXO 0748-676, a pair of resonance scattering lines consistent with Fe XXV and XXVI, gives the redshift  $z$  about 0.345, which constrains the mass  $M \geq 2.10 \pm 0.28 M_{\odot}$  and the radius  $R \geq 13.8 \pm 1.8$  km for the same object [18, 19]. In addition, the highest QPOs frequency 1330 Hz ever observed in 4U 0614+09 implies the mass  $M \lesssim 1.8 M_{\odot}$  and the radius  $R \lesssim 15$  km in this object [20]. Furthermore, modern observational soft X-ray data of cooling neutron stars associated with popular synthesis models' analysis reveal that an acceptable EoS shall not allow the direct Urca process [21] to occur in neutron stars with masses below  $1.5 M_{\odot}$  [22, 23, 24]. All of these indicate the strict constraints on the EoS of strongly interacting matter at high densities.

For the description of nuclear matter and finite nuclei, the relativistic many-body theory has achieved great success during the past years. One of the most successful representatives is the relativistic Hartree approach with the no-sea approximation, namely the relativistic mean field (RMF) theory [25, 26, 27]. With a limited number of free parameters including the meson masses and meson-nucleon coupling constants, the appropriate quantitative descriptions are obtained by RMF for both stable nuclei and exotic ones with large neutron excess [28, 29, 30, 31, 32, 33, 34, 35, 36, 37, 38, 39, 40, 41].

After the first theoretical calculations of the neutron star properties [42, 43], a plenty of theoretical prediction was made by both non-relativistic and relativistic approaches in the literature. At the early development of RMF, it was applied to evaluate the total mass and radius of neutron stars [44]. In the further development, the nuclear medium effects were taken into account by introducing the explicit or implicit density dependence into the meson-nucleon couplings, i.e., the density dependent meson-nucleon couplings [45, 46, 47] and the non-linear self-couplings of the meson fields [39, 48, 49], respectively. In Refs. [48, 50, 51], the effects of the non-linear self-coupling of  $\sigma$ ,  $\omega$  and  $\rho$  mesons were studied in describing the nuclear matter and neutron stars. On the other side, the influence on mean field potentials, saturation properties of nuclear matter, the EoS, the maximum mass and radius of neutron stars was systematically investigated with explicit density dependence in the meson-nucleon couplings [52, 53]. In addition, the consequences on compact star properties were studied with the inclusion of the degree of freedom of hyperons [54, 55, 56, 57]. With more accurate experimental data of the neutron radius of  $^{208}\text{Pb}$ , the correlation between the neutron skin thickness in finite nuclei and the symmetry energy of nuclear matter was discussed [58, 59, 60]. Further investigation in Ref. [61] proposed the relation between the neutron skin thickness of a heavy nucleus and neutron star radius that the larger neutron skin thickness prefers the larger neutron star radius, which implies the constraints on the EoS and on the cooling mechanism of neutron stars. Besides the RMF approach, the Dirac-Brueckner-Hartree-Fock (DBHF) and Brueckner-Hartree-Fock (BHF) with three-body force approaches were also applied to study

the neutron star properties with the realistic nucleon-nucleon interactions [62, 63, 64, 65, 66].

In the RMF approach, however, the Fock terms are neglected by the reason of simplicity. From the recent development on the relativistic Hartree-Fock theory, i.e., the density dependent relativistic Hartree-Fock (DDRHF) theory [67], it is found that the Fock terms are of special importance in determining the nuclear structure properties. Within DDRHF, the quantitatively comparable precision with RMF are obtained for the structure properties of nuclear matter and finite nuclei [67, 68]. Particularly, the new constituents introduced with the Fock terms, i.e., the  $\rho$ -tensor correlations and pion exchange potential, have brought significant improvement on the descriptions of the nuclear shell structures [68] and the evolutions [69]. Furthermore, the excitation properties and the non-energy weighted sum rules of the Gamow-Teller resonance and the spin-dipole resonance in the doubly magic nuclei have been well reproduced by RPA based on the DDRHF approach fully self-consistently [70]. Since the nuclear structure properties around the saturation density are evidently affected by the Fock terms, one might expect remarkable effects from the Fock terms on the nuclear matter properties in the high density region. Especially with the inclusion of the new ingredients in DDRHF, remarkable adjustment occurs on the coupling strength of the dominant mean fields ( $g_\sigma$  and  $g_\omega$ ), which may bring significant effects when exploring to the high density region.

In this paper, the properties of the static and  $\beta$ -equilibrium neutron stars without hyperons are studied within the DDRHF theory. As compared to the calculations of the RMF theory, the applicable ranges of density and isospin asymmetry are tested for DDRHF as well as the consistence with recent observational constraints of compact stars. In Section II is briefly introduced the formulism of DDRHF for nuclear matter and neutron star. In Section III, the calculated results and discussions are given, including the properties of symmetric and asymmetric nuclear matter in comparison with RMF in Section III A, in which the effects of Fock terms are studied in details, and the investigations of neutron stars in comparison with recent observational data in Section III B. Finally a summary is given.

## II. GENERAL FORMULISM OF DDRHF IN NUCLEAR MATTER

The relativistic Hartree-Fock (RHF) theory with density dependent meson-nucleon couplings, i.e., the DDRHF theory, was firstly introduced in Ref. [67], and the applications and corresponding effective interactions can be found in Refs. [67, 68, 69, 71]. In the following we just briefly recall the general formulism of DDRHF in nuclear matter and the application in neutron stars. More details of the RHF theory are referred to Refs. [67, 68, 72].

As the theoretical starting point, the Lagrangian density of DDRHF is constructed on the one-

boson exchange diagram of the NN interaction, which contains the degrees of freedom associated with the nucleon ( $\psi$ ), two isoscalar mesons ( $\sigma$  and  $\omega$ ), two isovector mesons ( $\pi$  and  $\rho$ ), and the photon ( $A$ ). Following the standard procedure in Ref. [72], one can derive the Hamiltonian in nucleon space as,

$$H = \int d^3x \bar{\psi} (-i\boldsymbol{\gamma} \cdot \boldsymbol{\nabla} + M) \psi + \frac{1}{2} \int d^3x d^4y \sum_{\phi} \bar{\psi}(x) \bar{\psi}(y) \Gamma_{\phi}(1, 2) D_{\phi}(1, 2) \psi(y) \psi(x), \quad (1)$$

where  $\phi = \sigma, \omega, \rho, \pi$  and  $A$ , and  $D_{\phi}$  denotes the propagators of mesons and photon. The interacting vertex  $\Gamma_{\phi}$  in the Hamiltonian (1) reads as,

$$\Gamma_{\sigma}(1, 2) \equiv -g_{\sigma}(1)g_{\sigma}(2), \quad (2a)$$

$$\Gamma_{\omega}(1, 2) \equiv +g_{\omega}(1)\gamma_{\mu}(1)g_{\omega}(2)\gamma^{\mu}(2), \quad (2b)$$

$$\Gamma_{\rho}(1, 2) \equiv +g_{\rho}(1)\gamma_{\mu}(1)\vec{\tau}(1) \cdot g_{\rho}(2)\gamma^{\mu}(2)\vec{\tau}(2), \quad (2c)$$

$$\Gamma_{\pi}(1, 2) \equiv -\frac{1}{m_{\pi}^2} [f_{\pi}\vec{\tau}\gamma_5\boldsymbol{\gamma} \cdot \boldsymbol{\nabla}]_1 \cdot [f_{\pi}\vec{\tau}\gamma_5\boldsymbol{\gamma} \cdot \boldsymbol{\nabla}]_2, \quad (2d)$$

$$\Gamma_A(1, 2) \equiv +\frac{e^2}{4} [\gamma_{\mu}(1 - \tau_3)]_1 [\gamma^{\mu}(1 - \tau_3)]_2. \quad (2e)$$

In current work, the  $\rho$ -tensor correlations are not enclosed. In the above expressions and following context, the isovectors are denoted by arrows and the space vectors are in bold type.

In general, the time component of the four-momentum carried by mesons are neglected on the level of the mean field approximation. This neglect has no consequence on the direct (Hartree) terms, while for the exchange (Fock) terms it amounts to neglect the retardation effects. The meson propagators are therefore of the Yukawa form, e.g., in the momentum representation,

$$D_{\phi}(1, 2) = \frac{1}{m_{\phi}^2 + \mathbf{q}^2}, \quad (3)$$

where the exchanging momentum  $\mathbf{q} = \mathbf{p}_2 - \mathbf{p}_1$ , and  $\phi = \sigma, \omega, \rho$  and  $\pi$ .

For the description of nuclear matter, the coulomb field thus could be neglected, and the momentum representation is generally adopted in the Hamiltonian. Due to time-reversal symmetry and rotational invariance, the self-energy  $\Sigma$  can be expressed as

$$\Sigma(p) = \Sigma_S(p) + \gamma_0 \Sigma_0(p) + \boldsymbol{\gamma} \cdot \hat{\mathbf{p}} \Sigma_V(p), \quad (4)$$

where  $\hat{\mathbf{p}}$  is the unit vector along  $\mathbf{p}$ , and the scalar component  $\Sigma_S$ , time component  $\Sigma_0$  and space component  $\Sigma_V$  of the vector potential are functions of the four-momentum  $p = (E(p), \mathbf{p})$  of nucleon. With the general form of the self-energy, the Dirac equation in nuclear matter can be written as,

$$(\boldsymbol{\gamma} \cdot \mathbf{p}^* + M^*) u(p, s, \tau) = \gamma_0 E^* u(p, s, \tau), \quad (5)$$

with the starred quantities,

$$\mathbf{p}^* = \mathbf{p} + \hat{\mathbf{p}}\Sigma_V(p), \quad (6a)$$

$$M^* = M + \Sigma_S(p), \quad (6b)$$

$$E^* = E(p) - \Sigma_0(p), \quad (6c)$$

which obey the relativistic mass-energy relation  $E^{*2} = \mathbf{p}^{*2} + M^{*2}$ . With this relationship, one can introduce the hatted quantities as

$$\hat{P} \equiv \frac{\mathbf{p}^*}{E^*}, \quad \hat{M} \equiv \frac{M^*}{E^*}. \quad (7)$$

With the momentum representation, the Dirac equation (5) can be formally solved and the Dirac spinors with positive energy read as

$$u(p, s, \tau) = \left[ \frac{E^* + M^*}{2E^*} \right]^{1/2} \begin{pmatrix} 1 \\ \frac{\boldsymbol{\sigma} \cdot \mathbf{p}^*}{E^* + M^*} \end{pmatrix} \chi_s \chi_\tau, \quad (8)$$

where  $\chi_s$  and  $\chi_\tau$  respectively denote the spin and isospin wave functions. The solution (8) is normalized as

$$u^\dagger(p, s, \tau)u(p, s, \tau) = 1. \quad (9)$$

The stationary solutions of the Dirac equation (5) consist of the positive and negative energy ones, and one can expand the nucleon field operator  $\psi$  in terms of Dirac spinors. Within the mean field approximation, the contributions from the negative energy states are neglected, i.e., the no-sea approximation. The nucleon field operate  $\psi$  is therefore expanded on the positive energy set as,

$$\psi(x) = \sum_{p,s,\tau} u(p, s, \tau) e^{-ipx} c_{p,s,\tau}, \quad (10a)$$

$$\psi^\dagger(x) = \sum_{p,s,\tau} u^\dagger(p, s, \tau) e^{ipx} c_{p,s,\tau}^\dagger. \quad (10b)$$

where  $c_{p,s,\tau}$  and  $c_{p,s,\tau}^\dagger$  are the annihilation and creation operators. With the no-sea approximation, the trial Hartree-Fock ground state can be constructed as,

$$|\Phi_0\rangle = \prod_{p,s,\tau} c_{p,s,\tau}^\dagger |0\rangle, \quad (11)$$

where  $|0\rangle$  is the vacuum state. The energy functional, i.e., the energy density in nuclear matter, is then obtained by taking the expectation of the Hamiltonian with respect to the ground state  $|\Phi_0\rangle$  in a given volume  $\Omega$ ,

$$\varepsilon = \frac{1}{\Omega} \langle \Phi_0 | H | \Phi_0 \rangle \equiv \langle T \rangle + \sum_{\phi} \langle V_{\phi} \rangle = \varepsilon_k + \sum_{\phi} (\varepsilon_{\phi}^D + \varepsilon_{\phi}^E), \quad (12)$$

where  $\phi = \sigma, \omega, \rho, \pi$ , and

$$\varepsilon_k = \sum_{p,s,\tau} \bar{u}(p, s, \tau)(\boldsymbol{\gamma} \cdot \mathbf{p} + M)u(p, s, \tau), \quad (13a)$$

$$\varepsilon_\phi^D = \frac{1}{2} \sum_{p_1, s_1, \tau_1} \sum_{p_2, s_2, \tau_2} \bar{u}(p_1, s_1, \tau_1) \bar{u}(p_2, s_2, \tau_2) \Gamma_\phi(1, 2) \frac{1}{m_\phi^2} u(p_2, s_2, \tau_2) u(p_1, s_1, \tau_1), \quad (13b)$$

$$\varepsilon_\phi^E = -\frac{1}{2} \sum_{p_1, s_1, \tau_1} \sum_{p_2, s_2, \tau_2} \bar{u}(p_1, s_1, \tau_1) \bar{u}(p_2, s_2, \tau_2) \Gamma_\phi(1, 2) \frac{1}{m_\phi^2 + \mathbf{q}^2} u(p_1, s_1, \tau_1) u(p_2, s_2, \tau_2). \quad (13c)$$

In the energy functional,  $\varepsilon_k$  denotes the kinetic energy density, and  $\varepsilon_\phi^D$  and  $\varepsilon_\phi^E$  respectively correspond to the direct (Hartree) and exchange (Fock) terms of the potential energy density. With the Dirac spinors in Eq. (8), one can obtain the contributions of the energy density from each channel. The kinetic energy density  $\varepsilon_k$  and the direct terms of the potential energy density  $\varepsilon_\phi^D$  can be written as,

$$\varepsilon_k = \sum_{i=n,p} \frac{1}{\pi^2} \int_0^{k_{F,i}} p^2 dp \left( p \hat{P} + M \hat{M} \right), \quad (14a)$$

$$\varepsilon_\sigma^D = -\frac{1}{2} \frac{g_\sigma^2}{m_\sigma^2} \rho_s^2, \quad (14b)$$

$$\varepsilon_\omega^D = +\frac{1}{2} \frac{g_\omega^2}{m_\omega^2} \rho_b^2, \quad (14c)$$

$$\varepsilon_\rho^D = +\frac{1}{2} \frac{g_\rho^2}{m_\rho^2} \rho_{b3}^2, \quad (14d)$$

where the scalar density  $\rho_s$ , baryonic density  $\rho_b$  and the third component  $\rho_{b3}$  read as,

$$\rho_s = \sum_{i=n,p} \frac{1}{\pi^2} \int_0^{k_{F,i}} p^2 dp \hat{M}(p), \quad (15a)$$

$$\rho_b = \sum_{i=n,p} \frac{k_{F,i}^3}{3\pi^2}, \quad (15b)$$

$$\rho_{b3} = \frac{k_{F,n}^3}{3\pi^2} - \frac{k_{F,p}^3}{3\pi^2}, \quad (15c)$$

with the fermi momentum  $k_{F,i}$  ( $i = n, p$ ).

TABLE I: The terms  $A_\phi, B_\phi$  and  $C_\phi$  in Eq. (16)

$\phi$	$A_\phi(p, p')$	$B_\phi(p, p')$	$C_\phi(p, p')$
$\sigma$	$g_\sigma^2 \Theta_\sigma(p, p')$	$g_\sigma^2 \Theta_\sigma(p, p')$	$-2g_\sigma^2 \Phi_\sigma(p, p')$
$\omega$	$2g_\omega^2 \Theta_\omega(p, p')$	$-4g_\omega^2 \Theta_\omega(p, p')$	$-4g_\omega^2 \Phi_\omega(p, p')$
$\rho$	$2g_\rho^2 \Theta_\rho(p, p')$	$-4g_\rho^2 \Theta_\rho(p, p')$	$-4g_\rho^2 \Phi_\rho(p, p')$
$\pi$	$-f_\pi^2 \Theta_\pi(p, p')$	$-f_\pi^2 \Theta_\pi(p, p')$	$2 \frac{f_\pi^2}{m_\pi^2} [(p^2 + p'^2) \Phi_\pi(p, p') - pp' \Theta_\pi(p, p')]$

Compared to the simple form of direct terms of the potential energy density, the exchange terms

are much more complicated. In the isoscalar channels ( $\phi = \sigma, \omega$ ), the expressions read as,

$$\varepsilon_\phi^E = \frac{1}{2} \frac{1}{(2\pi)^4} \sum_{\tau, \tau'} \delta_{\tau\tau'} \int pp' dp dp' \left[ A_\phi(p, p') + \hat{M}(p)\hat{M}(p')B_\phi(p, p') + \hat{P}(p)\hat{P}(p')C_\phi(p, p') \right]. \quad (16)$$

For the isovector channels ( $\phi = \rho, \pi$ ), one just needs to replace the isospin factor  $\delta_{\tau\tau'}$  by  $(2 - \delta_{\tau\tau'})$  in the above expression. The details of the terms  $A_\phi, B_\phi$  and  $C_\phi$  in Eq. (16) are shown in Table I, where the functions  $\Theta_\phi(p, p')$  and  $\Phi_\phi(p, p')$  are defined as,

$$\int d\Omega d\Omega' \frac{1}{m_\phi^2 + \mathbf{q}^2} = \frac{4\pi^2}{pp'} \ln \frac{m_\phi^2 + (p + p')^2}{m_\phi^2 + (p - p')^2} \equiv \frac{4\pi^2}{pp'} \Theta_\phi(p, p'), \quad (17a)$$

$$\int d\Omega d\Omega' \frac{\hat{\mathbf{p}} \cdot \hat{\mathbf{p}}'}{m_\phi^2 + \mathbf{q}^2} = \frac{4\pi^2}{pp'} \left\{ \frac{p^2 + p'^2 + m_\phi^2}{2pp'} \Theta_\phi(p, p') - 2 \right\} \equiv 2 \frac{4\pi^2}{pp'} \Phi_\phi(p, p'). \quad (17b)$$

From the potential energy densities in Eqs. (13b) and (13c), one can perform the following variation,

$$\Sigma(p)u(p, s, \tau) = \frac{\delta}{\delta \bar{u}(p, s, \tau)} \sum_{\sigma, \omega, \rho, \pi} [\varepsilon_\phi^D + \varepsilon_\phi^E], \quad (18)$$

and obtain the self-energy  $\Sigma(p)$  which includes the direct terms,

$$\Sigma_S^D = -\frac{g_\sigma^2}{m_\sigma^2} \rho_s, \quad (19a)$$

$$\Sigma_0^D = +\frac{g_\omega^2}{m_\omega^2} \rho_b + \frac{g_\rho^2}{m_\rho^2} \rho_{b3}, \quad (19b)$$

and the exchange terms,

$$\Sigma_{\tau, S}^E(p) = \frac{1}{(4\pi)^2 p} \int \hat{M}(p') p' dp' \sum_{\tau'} \left\{ \delta_{\tau\tau'} [B_\sigma + B_\omega]_{(p, p')} + (2 - \delta_{\tau\tau'}) [B_\rho + B_\pi]_{(p, p')} \right\}, \quad (20a)$$

$$\Sigma_{\tau, 0}^E(p) = \frac{1}{(4\pi)^2 p} \int p' dp' \sum_{\tau'} \left\{ \delta_{\tau\tau'} [A_\sigma + A_\omega]_{(p, p')} + (2 - \delta_{\tau\tau'}) [A_\rho + A_\pi]_{(p, p')} \right\}, \quad (20b)$$

$$\Sigma_{\tau, V}^E(p) = \frac{1}{(4\pi)^2 p} \int \hat{P}(p') p' dp' \sum_{\tau'} \left\{ \delta_{\tau\tau'} [C_\sigma + C_\omega]_{(p, p')} + (2 - \delta_{\tau\tau'}) [C_\rho + C_\pi]_{(p, p')} \right\}. \quad (20c)$$

In DDRHF, the explicit density dependence is introduced into the meson-nucleon couplings, i.e., the coupling constants  $g_\sigma, g_\omega, g_\rho$  and  $f_\pi$  are functions of the baryonic density  $\rho_b$ . In the isoscalar meson-nucleon coupling channels

following form,

$$g_\phi(\rho_b) = g_\phi(\rho_0) f_\phi(x), \quad (21)$$

where  $x = \rho_b/\rho_0$ , and  $\rho_0$  is the saturation density of nuclear matter, and the function  $f_\phi$  reads as

$$f_\phi(x) = a_\phi \frac{1 + b_\phi(x + d_\phi)^2}{1 + c_\phi(x + d_\phi)^2}. \quad (22)$$



In addition, five constraints,  $f_\phi(1) = 1$ ,  $f''_\sigma(1) = f''_\omega(1)$ , and  $f''_\phi(0) = 0$ , are introduced to reduce the number of free parameters. For the isovector channels, the exponential density dependence is adopted for  $g_\rho$  and  $f_\pi$

$$g_\rho(\rho_b) = g_\rho(0) e^{-a_\rho x}, \quad (23)$$

$$f_\pi(\rho_b) = f_\pi(0) e^{-a_\pi x}. \quad (24)$$

Due to the density dependence in meson-nucleon couplings, the additional contribution, i.e., the rearrangement term  $\Sigma_R$ , appears in the self-energy  $\Sigma$ . In nuclear matter, it can be written as,

$$\Sigma_R = \sum_{\phi=\sigma,\omega,\rho,\pi} \frac{\partial g_\phi}{\partial \rho_b} \sum_\tau \frac{1}{\pi^2} \int \left[ \hat{M}(p) \Sigma_{\tau,S}^\phi(p) + \Sigma_{\tau,0}^\phi(p) + \hat{P}(p) \Sigma_{\tau,V}^\phi(p) \right] p^2 dp. \quad (25)$$

From Eqs. (19), (20) and (25), the scalar component  $\Sigma_S$ , time component  $\Sigma_0$  and space component  $\Sigma_V$  of the vector potential in Eq. (4) can be obtained as,

$$\Sigma_S(p) = \Sigma_S^D + \Sigma_S^E(p), \quad (26a)$$

$$\Sigma_0(p) = \Sigma_0^D + \Sigma_0^E(p) + \Sigma_R, \quad (26b)$$

$$\Sigma_V(p) = \Sigma_V^E(p), \quad (26c)$$

from which the starred quantities in Eq. (6) and the hatted quantities in Eq. (7) can be obtained. Therefore, for nuclear matter with given baryonic density  $\rho_b$  and neutron-proton ratio  $N/Z$ , one can proceed the self-consistent iteration to investigate their properties: with the trial self-energies, one can determine the starred quantities, hatted quantities and calculate the scalar density, and then get the new self-energies for next iteration until the final convergence.

In this work, a neutron star is described as the  $\beta$ -stable nuclear matter system, which consists of not only neutrons and protons, but also leptons  $\lambda$  (mainly  $e^-$  and  $\mu^-$ ). The equations of motion for the leptons are the free Dirac equations and their densities can be expressed in terms of their corresponding Fermi momenta,  $\rho_\lambda = k_{F,\lambda}^3 / (3\pi^2)$  ( $\lambda = e^-, \mu^-$ ). The chemical potentials of nucleons and leptons satisfy the equilibrium conditions

$$\mu_p = \mu_n - \mu_e, \quad \mu_\mu = \mu_e, \quad (27)$$

where the chemical potentials  $\mu_n$ ,  $\mu_p$ ,  $\mu_\mu$  and  $\mu_e$  are determined by the relativistic energy-momentum relation at the momentum  $p = k_F$ ,

$$\mu_i = \Sigma_0(k_{F,i}) + E^*(k_{F,i}), \quad (28a)$$

$$\mu_\lambda = \sqrt{k_{F,\lambda}^2 + m_\lambda^2}, \quad (28b)$$

where  $i = n, p$  and  $\lambda = e^-, \mu^-$ . The lepton masses are respectively,  $m_e = 0.511$  MeV and  $m_\mu = 105.658$  MeV. In addition, the baryon density conservation and charge neutrality are imposed as

$$\rho_b = \rho_n + \rho_p, \quad \rho_p = \rho_\mu + \rho_e. \quad (29)$$

With these constraints, the energy density of neutron stars is then obtained as

$$\varepsilon_{\text{ns}} = \sum_{i=n,p,e,\mu} \varepsilon_{k,i} + \sum_{\phi=\sigma,\omega,\rho,\pi} (\varepsilon_{\phi}^D + \varepsilon_{\phi}^E). \quad (30)$$

Here the leptons are treated as the free Fermi gas by assuming that there are no interactions between leptons and nucleons or mesons and the kinetic energies of leptons can be expressed as,

$$\varepsilon_{k,\lambda} = \frac{1}{\pi^2} \int_0^{k_{F,\lambda}} p^2 dp \sqrt{p^2 + m_{\lambda}^2}. \quad (31)$$

With the thermodynamic relation, the pressure of the neutron star system can be obtained as,

$$P(\rho_b) = \rho_b^2 \frac{d}{d\rho_b} \frac{\varepsilon_{\text{ns}}}{\rho_b} = \sum_{i=n,p,e,\mu} \rho_i \mu_i - \varepsilon_{\text{ns}}. \quad (32)$$

At low density region ( $\rho_b < 0.08 \text{ fm}^{-3}$ ), instead of DDRHF calculations, the BPS[73] and BBP[74] models are chosen to provide the proper EoS.

The structure equations of a static, spherically symmetric, relativistic star are the Tolman-Oppenheimer-Volkov (TOV) equations [42, 43]. Taking  $c = G = 1$ , the TOV equations read as

$$\frac{dP}{dr} = - \frac{[P(r) + \varepsilon(r)] [M(r) + 4\pi r^3 P(r)]}{r [r - 2M(r)]}, \quad (33a)$$

$$\frac{dM}{dr} = 4\pi r^2 \varepsilon(r), \quad (33b)$$

where  $P(r)$  is the pressure of the star at radius  $r$ , and  $M(r)$  is the total star mass inside the sphere of radius  $r$ . Taking the equation of state of stellar matter as the input, one could proceed with the solution of TOV equations. The point  $R$ , at which the pressure vanishes, i.e.,  $P(R) = 0$ , defines the radius of the star and the corresponding  $M(R)$  is the gravitational mass. For a given EoS, the TOV equation has the unique solution which depends on a single parameter characterizing the conditions of matter at the center, such as the central density  $\rho(0)$  or the central pressure  $P(0)$ .

### III. RESULTS AND DISCUSSIONS

In this paper, the EoS and the neutron star properties are studied in DDRHF with the effective interactions PKO1, PKO2 and PKO3 [67, 69]. As shown in Table II, the coupling constant  $g_{\rho}(0)$  is fixed to the value in the free space in PKO1 whereas free to be adjusted in PKO2 and PKO3, and  $\pi$ -coupling is not included in PKO2. For comparison, the results calculated by RMF are also discussed. The effective interactions used in RMF calculations include the nonlinear self-coupling ones GL-97 [44], NL1 [75], NL3 [37], NLSH [76], TM1 [49] and PK1 [39], and the density-dependent ones TW99 [38], DD-ME1 [40], DD-ME2 [41] and PKDD [39].

TABLE II: The effective interactions PKO1, PKO2 and PKO3 of DDRHF[67], where the masses  $M = 938.9$  MeV,  $m_\omega = 783.0$  MeV,  $m_\rho = 769.0$  MeV and  $m_\pi = 138.0$  MeV.

	$m_\sigma$	$g_\sigma$	$g_\omega$	$g_\rho(0)$	$f_\pi(0)$	$a_\rho$	$a_\pi$	$\rho_0$
PKO1	525.769084	8.833239	10.729933	2.629000	1.000000	0.076760	1.231976	0.151989
PKO2	534.461766	8.920597	10.550553	4.068299	—	0.631605	—	0.151021
PKO3	525.667686	8.895635	10.802690	3.832480	1.000000	0.635336	0.934122	0.153006
	$a_\sigma$	$b_\sigma$	$c_\sigma$	$d_\sigma$	$a_\omega$	$b_\omega$	$c_\omega$	$d_\omega$
PKO1	1.384494	1.513190	2.296615	0.380974	1.403347	2.008719	3.046686	0.330770
PKO2	1.375772	2.064391	3.052417	0.330459	1.451420	3.574373	5.478373	0.246668
PKO3	1.244635	1.566659	2.074581	0.400843	1.245714	1.645754	2.177077	0.391293

## A. Properties of nuclear matter

### 1. Bulk properties

In Table III are shown the bulk quantities of nuclear matter at saturation point, i.e., the saturation density  $\rho_0$ , the binding energy per particle  $E_B/A$ , the incompressibility  $K$ , the symmetry energy  $J$  and the scalar mass  $M_S^*/M$ . The results calculated by RMF with both the nonlinear self-coupling effective interactions and the density-dependent ones, which have been studied systematically in Ref. [53], are included for comparison. The saturation density and the binding energy per particle given by DDRHF with PKO series are around  $0.152 \text{ fm}^{-3}$  and  $-16.0 \text{ MeV}$ , respectively, close to the values provided by RMF. The incompressibility  $K$  calculated by DDRHF with PKO1, PKO2 and PKO3 range from 249 to 262 MeV, close to the values given by RMF with density dependent effective interaction. In contrast, relatively large values of  $K$  (270~360 MeV) are obtained by RMF with the non-linear self-coupling of mesons, except GL-97 and NL1. For the symmetry energy  $J$ , the non-linear version of RMF also presents relatively large values (36~44 MeV) except GL-97, whereas the density-dependent version of RMF (except PKDD) provides comparative values (32~34 MeV) to DDRHF with PKO1, PKO2 and PKO3. For the scalar mass  $M_S^*$ , GL-97 gives the largest value and TW99 presents the smallest. The values given by DDRHF with PKO series are around 0.60, close to those by RMF with the non-linear self-couplings of mesons except GL-97, and systematically smaller values are obtained by RMF with the density dependent meson-nucleon couplings.

TABLE III: The saturation density  $\rho_0$  ( $\text{fm}^{-3}$ ), binding energy per particle  $E_B/A$  (MeV), incompressibility  $K$  (MeV), asymmetry energy coefficient  $J$  (MeV) and the scalar mass  $M_S^*/M$  of nuclear matter at saturation point.

	$\rho_0$	$E_B/A$	$K$	$J$	$M_S^*/M$
PKO1	0.1520	-15.996	250.239	34.371	0.5900
PKO2	0.1510	-16.027	249.597	32.492	0.6025
PKO3	0.1530	-16.041	262.469	32.987	0.5862
GL-97	0.1531	-16.316	240.050	32.500	0.7802
NL1	0.1518	-16.426	211.153	43.467	0.5728
NL3	0.1483	-16.249	271.730	37.416	0.5950
NLSH	0.1459	-16.328	354.924	36.100	0.5973
TM1	0.1452	-16.263	281.162	36.892	0.6344
PK1	0.1482	-16.268	282.694	37.642	0.6055
TW99	0.1530	-16.247	240.276	32.767	0.5549
DD-ME1	0.1520	-16.201	244.719	33.065	0.5780
DD-ME2	0.1518	-16.105	250.296	32.271	0.5722
PKDD	0.1496	-16.268	262.192	36.790	0.5712

## 2. Density dependence of the coupling constants

In DDRHF, the medium effects are evaluated by the density dependence in the meson-nucleon couplings. To understand the EoS, it is worthwhile to have a look at the density dependence of the coupling constants. In Fig. 1 are shown the coupling constants  $g_\sigma$ ,  $g_\omega$ ,  $g_\rho$  and  $f_\pi$  as functions of baryonic density  $\rho_b$ , where the results of the DDRHF effective interactions PKO1, PKO2 and PKO3 are given as compared to the RMF ones TW99, DD-ME2 and PKDD. As seen from Fig. 1, all the effective interactions present strong density dependence in the low density region ( $\rho_b < 0.2 \text{ fm}^{-3}$ ) for both isoscalar ( $\sigma$  and  $\omega$ ) and isovector ( $\rho$  and  $\pi$ ) meson-nucleon couplings. When density grows higher,  $g_\sigma$  and  $g_\omega$  in the left panels become stable. While due to the exponential density dependence, the isovector ones  $g_\rho$  and  $f_\pi$  tend to vanish (except  $g_\rho$  in PKDD and PKO1) as shown in the right panels. From this aspect, one can understand that the isoscalar mesons provide the dominant contributions in the high density region. Compared to the RMF effective interactions, PKO1, PKO2 and PKO3 have smaller  $g_\sigma$  and  $g_\omega$ . This is mainly due to the effects of Fock terms, which lead to the recombination of the ingredients in the nuclear interactions. With the inclusion of Fock terms, the nuclear attractions are shared by the Hartree terms of  $\sigma$ -coupling and the Fock terms of  $\omega$ -,  $\rho$ - and  $\pi$ -couplings, and the repulsions are contributed by the Hartree terms of  $\omega$ -coupling and the Fock terms of  $\sigma$ -coupling. While in RMF, the attraction and repulsion are

provided only by the Hartree terms of the  $\sigma$ - and  $\omega$ -couplings, respectively.

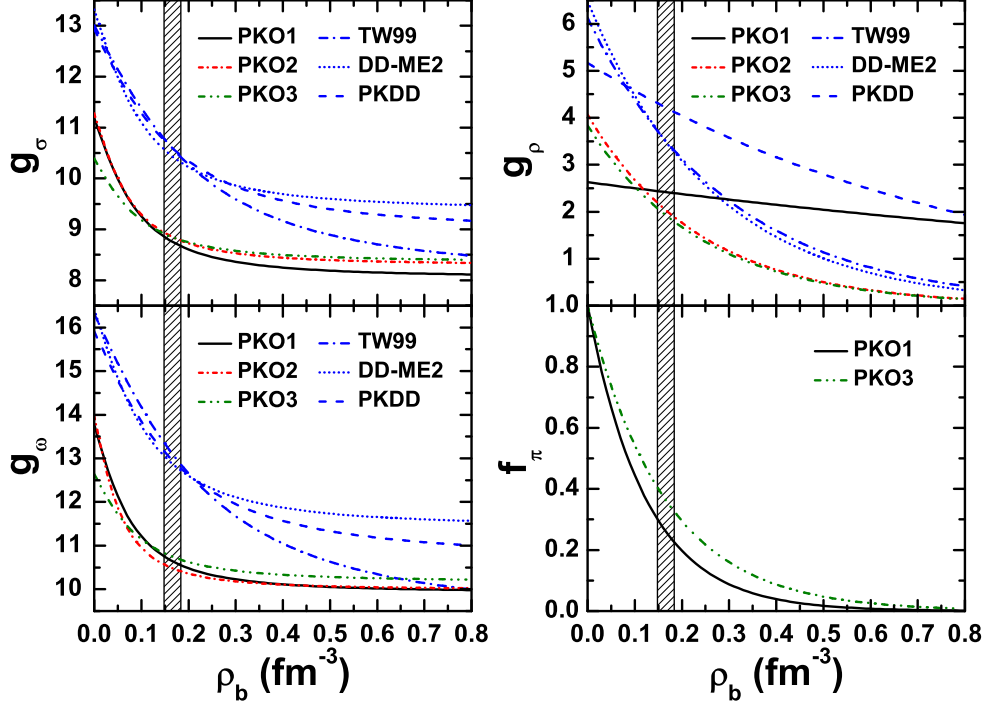


FIG. 1: (Color online) The coupling constants  $g_\sigma$ ,  $g_\omega$ ,  $g_\rho$  and  $f_\pi$  as functions of the baryonic density  $\rho_b$  (fm<sup>-3</sup>) for the DDRHF effective interactions PKO1, PKO2 and PKO3, and RMF ones PKDD, TW99 and DD-ME2. The shadowed area represents the empirical saturation region  $\rho_b = 0.166 \pm 0.018$  fm<sup>-3</sup>.

It is not enough to adjust the isospin properties only within the nuclear saturation region. It is expected that the investigations on the EoS at higher densities and neutron star properties could provide the additional constraint. For the isovector coupling constants in the right panels of Fig. 1, PKO1 and PKDD present slightly weak density dependence in  $g_\rho$  because of the fairly small density dependent parameter  $a_\rho$ . In analogy to  $g_\sigma$  and  $g_\omega$ , the RMF effective interactions give larger values of  $g_\rho$ . This is also due to the exchange contributions. In DDRHF, significant contributions to the isospin part of nuclear interaction are found in exchange terms of isovector mesons as well as isoscalar ones. It is different from the situation in RMF that the isospin properties are only described by the direct part of  $\rho$ -coupling. For the  $\pi$ -meson, the contribution in neutron stars is negligible since  $f_\pi$  tends to vanish at high densities.

### 3. Equations of state

The equations of state calculated by DDRHF with PKO1, PKO2 and PKO3 are shown in Fig. 2 and Fig. 3, respectively for the symmetric nuclear matter and pure neutron matter. The results calculated by RMF with TW99, DD-ME2 and PKDD are also shown for comparison. It is recommended to see Ref. [53] for the density dependence of the EoS on more RMF effective

interactions. Seen from these two figures, identical behaviors of the EoS are provided by all the effective interactions at low density region ( $\rho_b < \rho_0$ ) while in high density region exist pronounced deviations among different effective interactions.

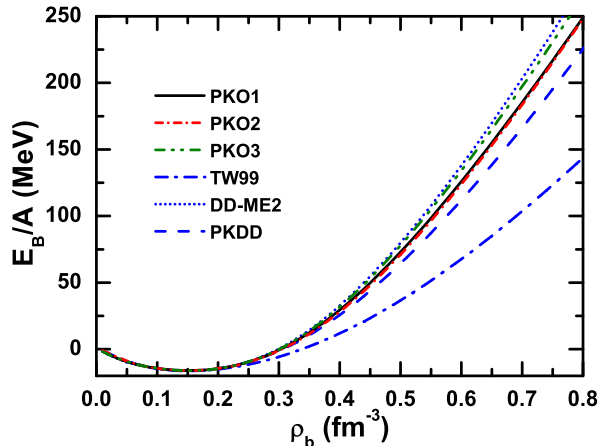


FIG. 2: (Color online) The binding energy per particle  $E_B/A$  as function of the baryonic density  $\rho_b$  for symmetric nuclear matter. The results are calculated by DDRHF with PKO1, PKO2 and PKO3, in comparison with those by RMF with TW99, DD-ME2 and PKDD.

For the symmetric nuclear matter in Fig. 2, DDRHF with PKO1, PKO2 and PKO3 provides similar EoS as RMF with PKDD and DD-ME2, whereas much softer EoS is obtained by RMF with TW99 when density grows high. For the pure neutron matter in Fig. 3, the curves can be classified into three groups according to the behaviors of the EoS at high density region. Among all the effective interactions, the DDRHF ones present the hardest equations of state and the RMF one TW99 gives the softest one, whereas DD-ME2 and PKDD provide similar equations of states, which lie between the hardest and softest. Since the DDRHF parameterizations were performed by fitting the properties of finite nuclei and nuclear matter around saturation point [67], which corresponds to the low density region, it becomes necessary to test the extrapolation of the effective interactions PKO1, PKO2 and PKO3 to high densities.

#### 4. Symmetry energy

The EoS property of isospin asymmetric nuclear matter is still ambiguous more or less. Different theoretical models predict quite different behaviors of the EoS for pure neutron matter. In most cases, it is due to the effective interactions obtained by fitting the properties of doubly magic nuclei, which have an isospin close to that of the symmetric nuclear matter. From this point of view, it becomes necessary to introduce the constraints, either from isospin asymmetric heavy-ion collisions experiments or from the data of nuclei with extreme isospin, into the fitting procedures of the effective interactions.

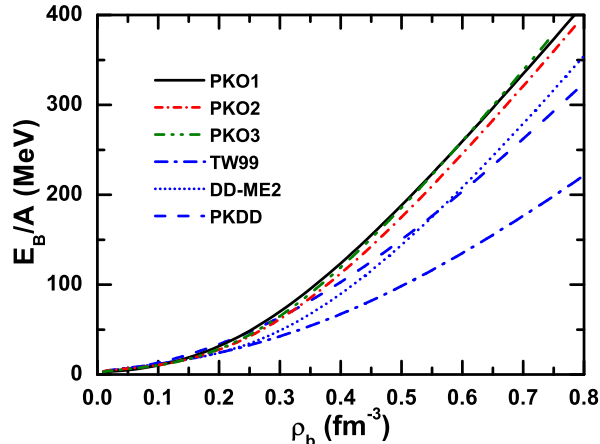


FIG. 3: (Color online) Similar to Fig. 2 but for pure neutron matter.

The symmetry energy is an important quantity to illustrate the property of asymmetric nuclear matter. In general, the energy per particle of asymmetric nuclear matter  $E(\rho_b, \beta)$  can be expanded in a Taylor series with respect to  $\beta$ ,

$$E(\rho_b, \beta) = E_0(\rho_b) + \beta^2 E_S(\rho_b) + \dots, \quad (34)$$

where  $\beta = 1 - 2\rho_p/\rho_b$  is the asymmetry parameter depending on the proton fraction. The function  $E_0(\rho_b)$  is the binding energy per particle in symmetric nuclear matter, and the symmetry energy  $E_S(\rho_b)$  ( $J = E_S(\rho_0)$ ) is denoted as

$$E_S(\rho_b) = \frac{1}{2} \left. \frac{\partial^2 E(\rho_b, \beta)}{\partial \beta^2} \right|_{\beta=0}. \quad (35)$$

The empirical parabolic law in Eq. (34) is confirmed to be reasonable in all the range of the asymmetry parameter values, while at high density deviation from such a behavior is found [77].

Fig. 4 shows the symmetry energy as a function of the baryon density  $\rho_b$ . The results are calculated by DDRHF with PKO1, PKO2 and PKO3, in comparison with those by RMF with TW99, DD-ME2 and PKDD. As shown in Fig. 4, both DDRHF and RMF effective interactions present identical behaviors of the symmetry energy at low densities ( $\rho < \rho_0$ ), while sizeable enhancements in high density region are obtained by DDRHF with PKO1, PKO2 and PKO3 as compared to the RMF results. Among the RMF calculations, PKDD shows harder behavior than DD-ME2 and TW99, which provide identical symmetry energy in the whole density region.

From the energy functional in nuclear matter in Eq. (12), one can obtain the contributions from different channels to the symmetry energy  $E_S$  as,

$$E_S = E_{S,k} + \sum_{\phi} (E_{S,\phi}^D + E_{S,\phi}^E), \quad (36)$$

where  $\phi = \sigma, \omega, \rho$  and  $\pi$ . In fact, the direct terms of  $\omega$ -meson coupling have no contribution to the symmetry energy because of the nature of isoscalar-vector coupling. It is also expected that the

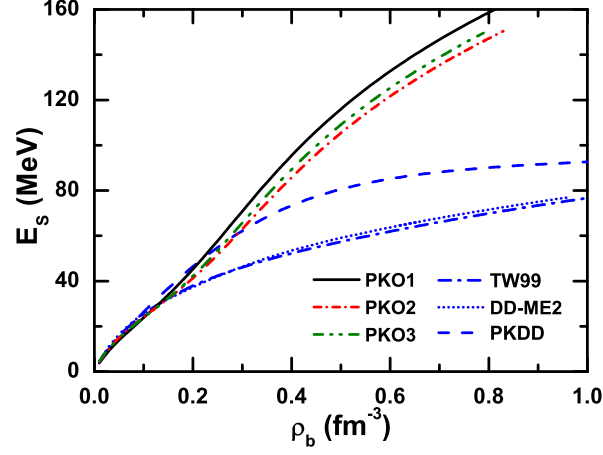


FIG. 4: (Color online) The nuclear symmetry energy  $E_S$  (MeV) as a function of the baryon density  $\rho_b$  ( $\text{fm}^{-3}$ ). The results are calculated by DDRHF with PKO1, PKO2 and PKO3, in comparison to those by RMF with TW99, DD-ME2 and PKDD.

one-pion exchange has minor effects since nuclear matter is a spin-saturated system. In Fig. 5, the contributions from different channels to the symmetry energy are shown as functions of the baryon density  $\rho_b$ . In the left panel are presented the contributions from the kinetic part and isoscalar channels, and only the results calculated by DDRHF with PKO1 are shown in comparison with those by RMF with PKDD and DD-ME2. The contributions from the  $\rho$ -meson coupling are shown in the right panel, including the results calculated by DDRHF with PKO1, PKO2 and PKO3, and RMF with PKDD, DD-ME2 and TW99.

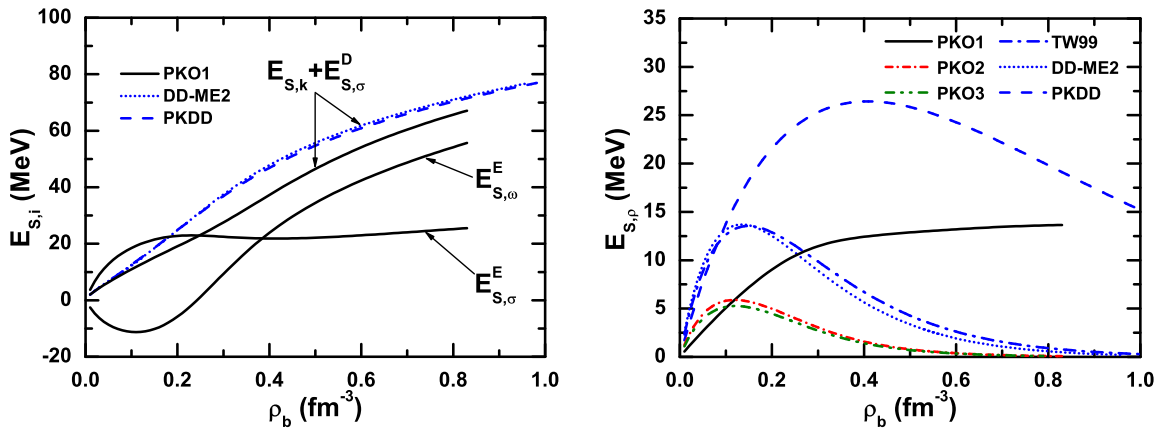


FIG. 5: (Color online) Contributions from different channels to the symmetry energy as a function of the baryon density  $\rho_b$ . Left panel gives the contributions from the kinetic energy and isoscalar channels, and the ones from  $\rho$ -meson are shown in the right panel. See text for details.

Within RMF, one can find that the kinetic part and the direct terms of  $\sigma$  coupling, i.e.,  $E_{S,k}$  and  $E_{S,\sigma}^D$ , provide the dominant contributions to the symmetry energy. As shown in the left panel of Fig. 5, PKDD and DD-ME2 give identical values of  $E_{S,k} + E_{S,\sigma}^D$ , and the deviation between



them appearing in Fig. 4 is mainly due to their contributions from the  $\rho$ -coupling as seen from the right panel of Fig. 5. In the left panel of Fig. 5, the values of  $E_{S,k} + E_{S,\sigma}^D$  given by the DDRHF calculations are found smaller than those of RMF with PKDD and DD-ME2. It is also seen that the Fock terms of  $\sigma$ - and  $\omega$ -couplings present significant contributions to the symmetry energy, which well interprets the stronger density dependence predicted by DDRHF than by RMF at the high density region (see Fig. 4). As seen from the left panel of Fig. 5, the values of  $E_{S,\sigma}^E$  increase rapidly in the low density region and tend to be stable about  $20 \sim 25$  MeV at high density. While the exchange terms of  $\omega$ -coupling provide negative contributions to the symmetry energy at low density and reach the minimum about  $-11$  MeV at  $\rho_b = 0.1 \text{ fm}^{-3}$ . After that the values of  $E_{S,\omega}^E$  grow up and become comparable to the values of  $E_{S,k} + E_{S,\sigma}^D$  at several times of the saturation density.

In the right panel of Fig. 5, the contributions of  $\rho$ -coupling, i.e.,  $E_{S,\rho} = E_{S,\rho}^D + E_{S,\rho}^E$ , are found to be important for the symmetry energy at low density region. When density goes high, the values of  $E_{S,\rho}$  given by all the effective interactions except PKO1 and PKDD tend to zero due to their strong exponential density dependence in  $\rho$ -nucleon coupling. Because of much smaller value of  $a_\rho$ , PKO1 presents larger contributions than PKO2 and PKO3 and contributes a value about  $10 \sim 15$  MeV in the high density region. Due to the same reason, PKDD also provides larger values of  $E_{S,\rho}$  than other two RMF effective interactions, and it reaches the maximum about 26 MeV at  $\rho_b \simeq 0.41 \text{ fm}^{-3}$ , then falls down slowly. Comparing the values of  $E_{S,\rho}$  given by PKO2 and PKO3 to those by DD-ME2 and TW99, the contribution of  $\rho$ -coupling  $E_{S,\rho}$  is depressed systematically in DDRHF. Such kind of depressions also exist between the results of PKO1 and PKDD, which are of similar density dependence in  $\rho$ -nucleon coupling. This could be understood from the fact that smaller values of  $g_\rho$  are obtained with the inclusion of Fock terms as seen in Fig. 1. In fact, not only the  $\rho$ -meson but all the mesons take part to the isospin properties and are in charge of producing the symmetry energy via the Fock channel.

Concluding the above discussions, one can find that the Fock terms play an important role in determining the density dependent behavior of the symmetry energy. It is then expected that the important constraints on the symmetry energy and the EoS of asymmetric nuclear matter could be obtained from the study of neutron stars.

## B. Properties of neutron star

In this work, the static and  $\beta$ -equilibrium assumptions are imposed for the description of neutron stars. With the density increasing, the high momentum neutrons will  $\beta$  decay into protons and electrons, i.e.,  $n \leftrightarrow p + e^- + \bar{\nu}_e$ , until the chemical potentials satisfy the equilibrium  $\mu_p = \mu_n - \mu_e$ .

When the chemical potential of electron  $\mu_e$  reaches the limit of the muon mass, the lepton  $\mu^-$  will appear. The reaction  $e^- \leftrightarrow \mu^- + \bar{\nu}_\mu + \nu_e$  implies the equilibrium between the  $e^-$  and  $\mu^-$  chemical potentials, i.e.,  $\mu_e = \mu_\mu$ .

### 1. Density distribution

To keep the equilibrium among the particle chemical potentials, protons, electrons and muons will appear with the density increasing in neutron stars. In Fig. 6 are shown the neutron, proton, electron and muon densities in neutron stars as functions of the baryon density. The results are calculated by DDRHF with PKO1, PKO2 and PKO3, in comparison to those by RMF with TW99, DD-ME2 and PKDD. The density distribution of various components in RMF with both the nonlinear self-coupling effective interactions and the density-dependent ones have been studied systematically in Ref. [53]. As seen from Fig. 6, the thresholds of  $\mu^-$  occurrence predicted by different effective interactions are very close to each another, roughly around  $\rho_b = 0.12 \text{ fm}^{-3}$ . It is shown that all the densities keep increasing monotonously with respect to the baryonic density  $\rho_b$ . Similar as the situation in the EoS of nuclear matter, different effective interactions present identical trends at low densities ( $\rho_b < \rho_0$ ), while remarkable deviations exist in high density region between the DDRHF and RMF predictions. Seen from Fig. 6, the results given by different effective interactions can be classified into three groups, the DDRHF ones, PKDD, and the RMF ones DD-ME2 and TW99. For the proton, electron and muon densities, the strongest density dependence is presented by DDRHF with PKO1, PKO2 and PKO3, while the softest behaviors are provided by RMF with DD-ME2 and TW99. In contrast, the softest behavior on neutron density is predicted by the DDRHF effective interactions, whereas TW99 and DD-ME2 present the hardest. This kind of reversion can be well understood from the relations in Eq. (29) among the densities.

It is known that the density fractions of each components in neutron stars are rather sensitive to the symmetry energy, as illustrated by associating Fig. 6 with Fig. 4. Due to the strong effects from the exchange terms of  $\omega$ -coupling in high density region (see Fig. 5), DDRHF with PKO1, PKO2 and PKO3 shows stronger density dependence on the symmetry energy and then are obtained the harder behaviors on the proton, electron and muon density distributions, as compared to the RMF calculations. For the deviations between different effective interactions within one theoretical model, e.g., between PKDD and DD-ME2, they are mainly due to the  $\rho$ -coupling as shown in the right panel of Fig. 5, where the  $\rho$ -meson coupling of PKDD shows larger contributions to the symmetry energy. As a conclusion, the harder behavior on the symmetry energy at high densities, more difficult the system becomes asymmetric and more easier neutrons decay into protons and electrons, which leads to smaller neutron abundance and larger proton, electron and

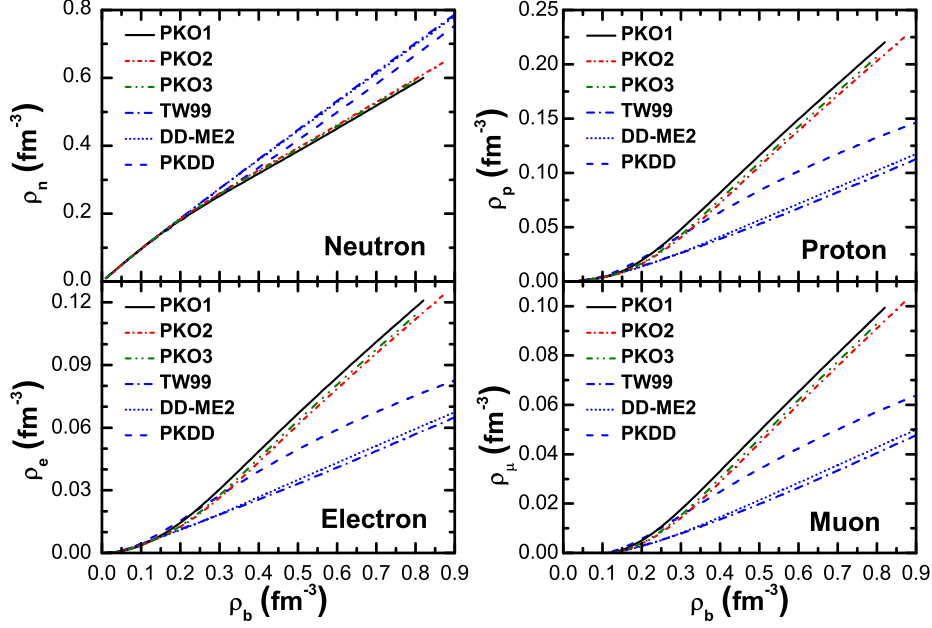


FIG. 6: (Color online) The neutron (up-left panel), proton (up-right panel), electron (lower-left panel) and muon (lower-right panel) densities in neutron star matter as functions of the baryon density  $\rho_b$  ( $\text{fm}^{-3}$ ). The results are calculated by DDRHF with PKO1, PKO2 and PKO3, in comparison to those by RMF with TW99, DD-ME2 and PKDD.

muon abundances in neutron stars.

## 2. Proton fraction and direct Urca constraint

From the density distributions in Fig. 6, one can extract the proton fraction  $x = \rho_p / (\rho_p + \rho_n)$  within the range of density of neutron stars. Fig. 7 shows the proton fraction  $x$  as a function of baryonic density  $\rho_b$ , where the results calculated by DDRHF with PKO series are presented in comparison to those by RMF with TW99, DD-ME2 and PKDD. Due to the stiff behavior on the symmetry energy (see Fig. 4), stronger density dependence of the proton fraction  $x$  in neutron star matter is obtained by DDRHF than RMF as shown in Fig. 7.

The cooling mechanism of neutron stars, which is sensitive to the proton fraction, could bring significant information of asymmetric nuclear EoS. Direct Urca (DU) processes  $n \rightarrow p + e^- + \bar{\nu}_e$  and  $p + e^- \rightarrow n + \nu_e$  lead the star to cool off rapidly by emitting the thermal neutrinos. The threshold of the proton fraction  $x^{DU}$  for the DU process occurring can be easily found as  $11.1\% \leq x^{DU} \leq 14.8\%$  with the momentum conservation and charge neutrality [21, 24]. Seen From Fig. 7, the critical density  $\rho^{DU}$  for the DU process occurring depends on the EoS. Once the critical density  $\rho^{DU}$  is reached in the center of a neutron star for a given EoS, the star will be efficiently cooled via the DU process. It is found that the values of  $x^{DU}$  given by DDRHF calculations correspond to fairly low

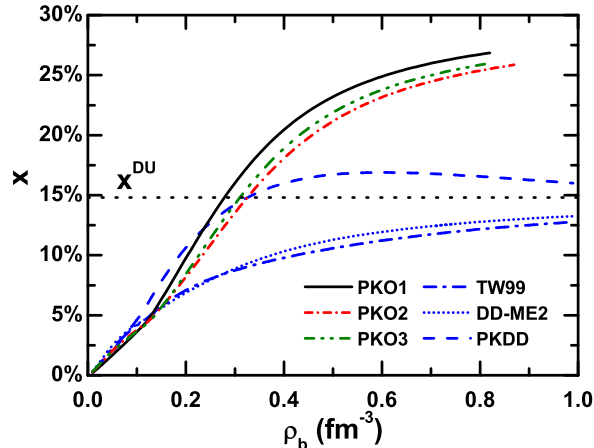


FIG. 7: (Color online) Proton fractions  $x = \rho_p/(\rho_p + \rho_n)$  in neutron star matter for different DDRHF and DDRMF effective interactions. The dotted line labeled with  $x^{DU}$  is threshold for happening direct Urca process. Here  $x^{DU} = 14.8\%$  is taken by assuming muons in the massless limit.

critical densities while the results calculated by RMF with TW99 and DD-ME2 do not support the DU process occurring at all. The DU critical star masses  $M^{DU}$  and corresponding central densities  $\rho^{DU}(0)$  are marked in Fig. 9 by filled squares.

According to the analysis in Refs. [22, 23, 24], if the DU process is taken as a possible mechanism for neutron star cooling, an acceptable EoS shall not allow it to occur in neutron stars with masses below  $1.5 M_\odot$ , otherwise it will be in disagreement with modern observational soft X-ray data in the temperature-age diagram. As a weaker constraint, the limit  $M^{DU} > 1.35 M_\odot$  could be applied. From the mass limit  $M^{DU}$ , are then obtained the constraint over the EoS that the density dependence of the symmetry energy should not be too strong, and probably not too weak, either. In Table IV, are given the critical neutron star mass  $M^{DU}$  and central densities  $\rho^{DU}(0)$  from the DDRHF and RMF calculations, which support the occurrence of the DU cooling process in stars.

Seen from Table IV, rather small mass limits  $M^{DU}$  are obtained by RMF with the non-linear self-coupling of mesons while the DDRHF calculations with PKO2 and PKO3 provide larger values of  $M^{DU}$ , which are very close to the limit  $1.5 M_\odot$  mentioned above and satisfy the weak constraint that  $M^{DU} > 1.35 M_\odot$ . For the calculation with PKO1, the DU cooling process will occur at the fairly low mass  $1.20 M_\odot$  and central density  $\rho^{DU} \simeq 0.28 \text{ fm}^{-3}$ , which can be interpreted by the contributions of the  $\rho$ -meson coupling to the symmetry energy. For the  $E_{S,\rho}$  in the right panel of Fig. 5, the  $\rho$ -meson coupling in PKO1 still has remarkable effects in the high density region due to the weak density dependence of  $g_\rho$  (see Fig. 1). Due to the same reason, the RMF calculation with PKDD also support the DU cooling process to occur at a low mass limit  $1.26 M_\odot$ . In contrast, as seen in Fig. 7, the occurrence of the DU cooling process is not supported at all by the RMF calculations with TW99 and DD-ME2 as well as DD-ME1. It is expected that the occurrence of

the DU process could be introduced as a possible constraint in the future parameterizations of both DDRHF and RMF, e.g., for the  $\rho$ -meson coupling ( $g_\rho(0)$  and  $a_\rho$ ).

TABLE IV: Critical neutron star masses  $M^{\text{DU}}$  and central densities  $\rho^{\text{DU}}(0)$  for the occurrence of the DU cooling process and the criterion of the DU constraint given by both DDRHF and RMF effective interactions. Fulfillment (violation) of a constraint is indicated with +(-).

	PKO1	PKO2	PKO3	GL-97	NL1	NL3	NLSH	TM1	PK1	PKDD
$M^{\text{DU}} [M_\odot]$	1.20	1.45	1.43	1.10	0.75	1.01	1.20	0.96	0.94	1.26
$\rho^{\text{DU}}(0) [\text{fm}^{-3}]$	0.28	0.33	0.31	0.33	0.20	0.23	0.24	0.24	0.23	0.33
$M^{\text{DU}} \geq 1.5 M_\odot$	-	-	-	-	-	-	-	-	-	-
$M^{\text{DU}} \geq 1.35 M_\odot$	-	+	+	-	-	-	-	-	-	-

### 3. Pressure and maximum mass of neutron star

In Fig. 8, the pressures of neutron star matter calculated by DDRHF effective interactions are shown as functions of the baryonic density  $\rho_b$ . The results with RMF ones GL-97, NL3, TW99 in Ref. [53] and also PK1, DD-ME2, PKDD have been included for comparison. It is found that PKO1, PKO2 and PKO3 provide identical behaviors with each another over the density dependence of the pressure, which are also close to the behaviors predicted by RMF with PKDD and DD-ME2. Among all the DDRHF and RMF calculations, NL3 provides the strongest density dependence and the softest are presented by GL-97. The behaviors given by PK1 and TW99 lie between the results of DDRHF with PKO series and RMF with GL-97.

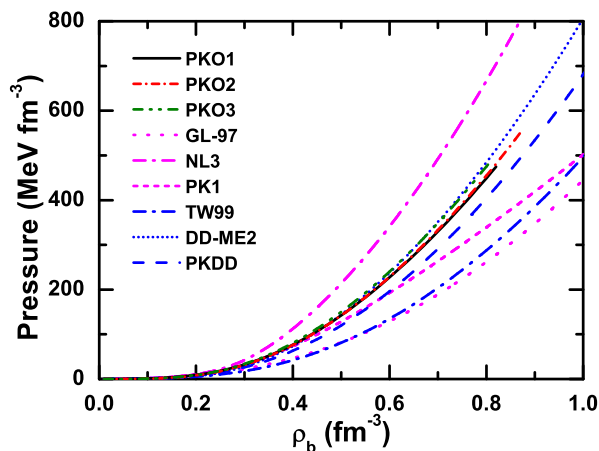


FIG. 8: (Color online) The pressure of neutron star matter as a function of the baryon density  $\rho_b$  ( $\text{fm}^{-3}$ ). The results are calculated by DDRHF with PKO1, PKO2, and PKO3, in comparison to those by RMF with GL-97, NL3, PK1, TW99, DD-ME2, and PKDD.

The variation of the pressure with respect to density is essential to understand the structure of

neutron stars. Stronger density dependence of the pressure at high densities would lead to larger value of maximum mass for neutron stars that can be sustained against collapse. In Fig. 9, the neutron star masses calculated by DDRHF with PKO1, PKO2, and PKO3 are shown as functions of the central density  $\rho(0)$ . For comparison, are also shown the results calculated by RMF with GL-97, NL3, PK1, TW99, DD-ME2, and PKDD, and one could refer to Ref. [53] for more studies with a variety of RMF effective interactions. From Fig. 9, it is found that the maximum masses given by the DDRHF calculations lie between  $2.4 M_\odot$  and  $2.5 M_\odot$  with the central densities around  $0.80 \text{ fm}^{-3}$ , which are close to the prediction of RMF with DD-ME2. Notice that these values are also compatible to the observational constraint ( $M = 2.08 \pm 0.19 M_\odot$ ) from PSR B1516+02B [14]. In Table V are shown the maximum mass limits  $M_{\text{max}}$  and the corresponding central densities  $\rho_{\text{max}}(0)$  extracted from Fig. 9. As consistent with the description of the pressure, the non-linear RMF effective interaction NL3 presents a rather large value of the maximum mass  $M_{\text{max}} = 2.78 M_\odot$  with small central density  $\rho_{\text{max}}(0) = 0.67 \text{ fm}^{-3}$ , while the smallest  $M_{\text{max}}$  and the largest  $\rho_{\text{max}}(0)$  are obtained by RMF with GL-97 and TW99, which gives the softest behaviors of the pressure (see Fig. 8). Seen from Table V, the values of  $M_{\text{max}}$  given by all the effective interactions are in the appropriate agreements with the constraint on the maximum mass from PSR B1516+02B.

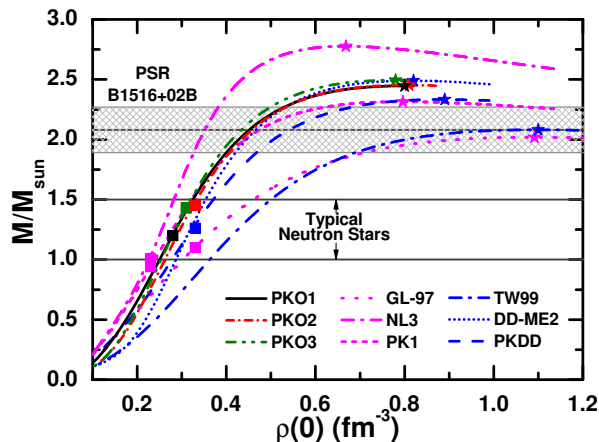


FIG. 9: (Color online) Neutron star mass as a function of the central density for different DDRHF and RMF effective interactions. Filled stars denote the maximum mass configurations, filled squares mark the critical mass  $M^{\text{DU}}$  and central density values  $\rho^{\text{DU}}(0)$  where the DU cooling process becomes possible. The light grey horizontal bands around  $2.08 M_\odot$  denote the  $1\sigma$  confidence level for the mass measurement of PSR B1516+02B [14]. The mass region of typical neutron stars is between  $1.0 M_\odot$  and  $1.5 M_\odot$ .

#### 4. Mass-Radius relation and observational constraint

Recent astronomic observations also provide the constraints on the mass-radius relation of neutron stars. In this paper, four typical observations are adopted to test the theoretical calculations.

TABLE V: Maximum mass limits  $M_{\max}$  ( $M_{\odot}$ ), the corresponding central densities  $\rho_{\max}(0)$  ( $\text{fm}^{-3}$ ) and radii  $R(M_{\max})$  (km) for neutron stars calculated by DDRHF and RMF effective interactions. The radii (km) for  $1.4 M_{\odot}$  neutron stars are shown as well.

	PKO1	PKO2	PKO3	GL-97	NL1	NL3	NLSH	TM1	PK1	TW99	DD-ME1	DD-ME2	PKDD
$M_{\max}$	2.45	2.45	2.49	2.02	2.81	2.78	2.80	2.18	2.32	2.08	2.45	2.49	2.33
$\rho_{\max}(0)$	0.80	0.81	0.78	1.09	0.66	0.67	0.65	0.85	0.80	1.10	0.84	0.82	0.89
$R(M_{\max})$	12.4	12.3	12.5	10.9	13.4	13.3	13.5	12.4	12.7	10.7	11.9	12.1	11.8
$R(1.4M_{\odot})$	14.1	13.8	13.9	13.3	14.7	14.7	14.9	14.4	14.5	12.4	13.2	13.3	13.7

1. The large radiation radius  $R_{\infty} = 16.8$  km ( $R_{\infty} = R/\sqrt{1 - 2GM/Rc^2}$ ) from the isolated neutron star RX J1856 [16].
2. The redshift  $z \simeq 0.345$ , the mass  $M \geq 2.10 \pm 0.28 M_{\odot}$  and the radius  $R \geq 13.8 \pm 1.8$  km constraints in LMXBs EXO 0748-676 [18, 19].
3.  $M \lesssim 1.8 M_{\odot}$  and  $R \lesssim 15$  km constraints from the highest frequency of QPOs 1330 Hz ever observed in 4U 0614+09 [20].
4. Several neutron stars in LMXBs have gravitational masses between  $1.9 M_{\odot}$  and possibly  $2.1 M_{\odot}$  from the QPOs data analysis in LMXBs 4U 1636-536 [13].

In Fig. 10 are shown the mass-radius relations of neutron stars calculated by DDRHF with PKO1, PKO2 and PKO3, and RMF with GL-97, NL3, PK1, TW99, DD-ME2 and PKDD. The results with more RMF effective interactions have been investigated in Ref. [53]. For comparison, the selected observational constraints are marked with different colors and grids as shown in Fig. 10. The causality limit that  $\sqrt{\partial p/\partial \varepsilon} \leq 1$  results in  $R > 2.9GM/c^2$  [78, 79] and the corresponding region in Fig. 10 is marked in black. Compared to all the observational limits, it is found that better agreements are obtained by the DDRHF effective interactions than the RMF ones. Among the RMF results, GL-97 is excluded by the limits from RX J1856, and TW99 is excluded by the limits from both RX J1856 and EXO 0748-676, while NL3 could not fulfil the constraint from 4U 0614+09. If upper mass limit  $2.1 M_{\odot}$  is taken in 4U 1636-536, GL-97 and TW99 (just a marginal cover) is not satisfied either. The detailed criteria of the M-R constraints are presented in Table VI. It is shown that the predictions given by DDRHF with PKO series and RMF with PK1, TM1, DD-ME1, DD-ME2 and PKDD fulfill all the M-R constraints.

In Refs. [58, 59], the radius of neutron stars with the mass  $1.4 M_{\odot}$  was found to be correlated with the neutron skin thickness of  $^{208}\text{Pb}$  as well as the symmetry energy. If the observation can limit the radius of neutron stars to a narrow range, a strong constraint can be imposed on the symmetry energy. On the other hand, if the neutron skin thickness of  $^{208}\text{Pb}$  or the symmetry energy



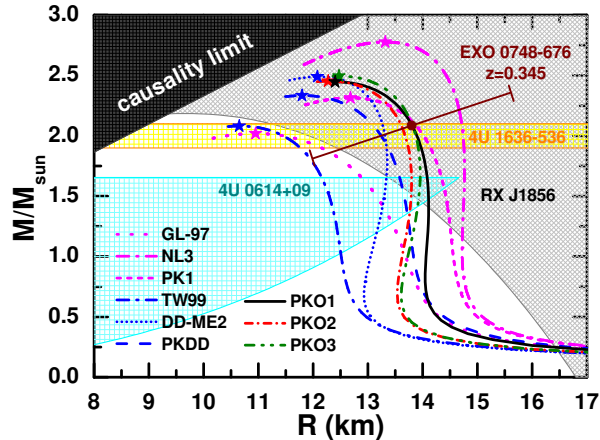


FIG. 10: (Color online) Mass-radius relations of neutron stars provided by the DDRHF and RMF calculations and the corresponding maximum masses are marked in filled star symbols. For comparison, are also shown the four separate observational constraints from RX J1856 (gray grided region), 4U 0614+09 (cyan grided area), 4U 1636-536 (yellow grided area) and EXO 0748-676 (wine line for  $1\sigma$  error). The black region is excluded by causality that  $R > 2.9GM/c^2$  [78, 79]. See the text for details.

TABLE VI: The criterion of the M-R constraints: (1) the isolated neutron star RX J1856, (2) EXO 0748-676, (3) the low-mass X-ray binary 4U 0614+09, (4-u) 4U 1636-536 with its upper mass limits, and (4-l) 4U 1636-536 with its lower mass limits. Fulfillment (violation) of a constraint is indicated with +(-) and the marginal cover is marked with  $\Delta$ . See the text for details.

	PKO1	PKO2	PKO3	GL-97	NL1	NL3	NLSH	TM1	PK1	TW99	DD-ME1	DD-ME2	PKDD
1	+	+	+	-	+	+	+	+	+	-	+	+	+
2	+	+	+	+	+	+	+	+	+	$\Delta$	+	+	+
3	+	+	+	+	$\Delta$	$\Delta$	-	+	+	+	+	+	+
4-u	+	+	+	-	+	+	+	+	+	$\Delta$	+	+	+
4-l	+	+	+	+	+	+	+	+	+	+	+	+	+

could be precisely determined from the terrestrial experiments, it will be helpful to understand the neutron star structure and rule out some EoSs for the neutron star matter. As seen in Fig. 10 and Table V, although several equations of state provide similar maximum masses, they still show some discrepancy for the radius of neutron stars with the mass  $1.4 M_{\odot}$ . In Table V, the DDRHF interactions predict this radius in a range from 13.8 km to 14.1 km, while the nonlinear RMF one NLSH gives the largest value 14.9 km, and the density dependent RMF one TW99 shows the smallest 12.4 km. All the calculated results except TW99 are coincident with the X-ray spectral analysis of the quiescent LMXB X7 in the globular cluster 47 Tuc, which requires a rather large radius of  $14.5^{+1.8}_{-1.6}$  km for  $1.4 M_{\odot}$  compact stars [17].



#### IV. SUMMARY

In this paper, the equations of state for symmetric nuclear matter, pure neutron matter and  $\beta$ -stable neutron star matter have been studied within the density dependent relativistic Hartree-Fock (DDRHF) theory with PKO1, PKO2 and PKO3. Substantial effects from the Fock terms are found in describing the asymmetric nuclear matter at high densities. Due to the contributions from the Fock terms of  $\sigma$ - and  $\omega$ -couplings, stronger density dependence on the symmetry energy is obtained from DDRHF at high densities, as compared to the RMF calculations with the density dependent meson-nucleon couplings. Because of the weak density dependence of  $g_\rho$  in PKO1, which induces remarkable contributions from the  $\rho$ -meson coupling to the symmetry energy, PKO1 shows stronger density dependence on the symmetry energy than both PKO2 and PKO3. With the obtained equations of state for  $\beta$ -stable nuclear matter, the properties of neutron stars are investigated within the DDRHF theory for the first time and the recent observational constraints of compact stars are also introduced to test the applicability of the DDRHF models.

Due to the extra enhancement from the  $\sigma$  and  $\omega$  exchange terms on the symmetry energy, large proton fractions in neutron stars are predicted by the DDRHF calculations, which affects essentially the cooling process of the star. For the DU process occurring, DDRHF with PKO2 and PKO3 gives critical neutron star mass  $\sim 1.45 M_\odot$ , which are close to the limit  $1.5 M_\odot$  from the modern soft X-ray data analysis in the temperature-age diagram and fulfil the weaker constraint  $1.35 M_\odot$ . In contrast, fairly small mass limits are presented by the calculations of DDRHF with PKO1, RMF with the non-linear self-couplings of mesons, and RMF with PKDD, mainly due to their stronger  $\rho$ -coupling contributions to the symmetry energy at high densities. Different from these two cases, the RMF calculations with TW99, DD-ME1 and DD-ME2 do not support the occurrence of DU process in neutron stars at all. In addition, the radii of  $1.4 M_\odot$  neutron stars are correlated with the symmetry energy as well. In general, stronger density dependence on the symmetry energy leads to larger radius for  $1.4 M_\odot$  neutron star. The radii given by the DDRHF calculations lie between 13.8 and 14.1 km, larger than the RMF calculations with the density-dependent meson-nucleon couplings, and smaller than the ones with the non-linear self-couplings of mesons except GL-97.

For the maximum masses and central densities of neutron stars, they are tightly correlated with the behavior of the pressure with respect to the density. Due to the similar density dependent behaviors of the pressure, identical maximum masses ( $\sim 2.5 M_\odot$ ) of neutron stars are found in the calculations of DDRHF, and RMF with DD-ME1 and DD-ME2, as well as the central densities around  $0.80 \text{ fm}^{-3}$ . The results are in reasonable agreement with high pulsar mass  $2.08 \pm 0.19 M_\odot$  from PSR B1516+02B recently reported. The mass-radius relations of neutron stars determined

by the DDRHF calculations are also consistent with the observational data from thermal radiation measurement in the isolated neutron star RX J1856, QPOs frequency limits in LMXBs 4U 0614+09 and 4U 1636-536, and the redshift limit determined in LMXBs EXO 0748-676, which are only partially satisfied in the RMF calculations with GL-97, NL1, NL3, NLSH and TW99.

### Acknowledgments

The authors thank H.-J. Schulze for the stimulating discussions and D. Blaschke for communications about the observational constraints of compact stars. This work is partly supported by Major State Basic Research Development Program (2007CB815000), the National Natural Science Foundation of China (10435010, 10775004, and 10221003) and Asia-Europe Link Program in Nuclear Physics and Astrophysics (CN/ASIA-LINK/008 094-791).

- 
- [1] F. Weber, *Pulsars as Astrophysical Laboratories for Nuclear and Particle Physics* (IOP, Bristol, 1999).
  - [2] S. L. Shapiro and S. A. Teukolsky, *Black Holes, White Dwarfs, and Neutron Stars, The Physics of the Compact Objects* (Wiley, New York, 1983).
  - [3] F. Weber, R. Negreiros, P. Rosenfield, and M. Stejner, *Prog. Part. Nucl. Phys.* **59**, 94 (2007).
  - [4] P. Danielewicz, R. Lacey, and W. G. Lynch, *Science* **298**, 1592 (2002).
  - [5] C. Fuchs, *Phys. Rep.* **56**, 1 (2006).
  - [6] B.-A. Li, L.-W. Chen, and C. M. Ko, *Phys. Rep.* **464**, 113 (2008).
  - [7] L. Landau, *Physikalische Zeitschrift der Sowjetunion* **1**, 285 (1932).
  - [8] W. Baade and F. Zwicky, *Proc. Nat. Acad. Sci. U.S.A.* **20**, 255 (1934).
  - [9] A. Hewish, S. J. Bell, J. D. H. Pilkington, P. F. Scott, and R. A. Collins, *Nature* **217**, 709 (1968).
  - [10] F. Pacini, *Nature* **216**, 567 (1967).
  - [11] J. M. Lattimer and M. Prakash, *Science* **304**, 536 (2004).
  - [12] J. M. Lattimer and M. Prakash, *Phys. Rep.* **442**, 109 (2007).
  - [13] D. Barret, J.-F. Olive, and M. C. Miller, *Mon. Not. Roy. Astron. Soc.* **361**, 855 (2005).
  - [14] P. C. C. Freire, A. Wolszczan, M. van den Berg, and J. W. T. Hessels, *Astrophys. J.* **679**, 1433 (2008).
  - [15] P. C. C. Freire, S. M. Ransom, S. Bégin, I. H. Stairs, J. W. T. Hessels, L. H. Frey, and F. Camilo, *Astrophys. J.* **675**, 670 (2008).
  - [16] J. E. Trümper, V. Burwitz, F. Haberl, and V. E. Zavlin, *Nucl. Phys. Proc. Suppl.* **132**, 560 (2004).
  - [17] C. O. Heinke, G. B. Rybicki, R. Narayan, and J. E. Grindlay, *Astrophys. J.* **644**, 1090 (2006).
  - [18] J. Cottam, F. Paerls, and M. Mendez, *Nature* **420**, 51 (2002).
  - [19] F. Özel, *Nature* **441**, 1115 (2006).
  - [20] M. C. Miller, *AIP Conf. Proc.* **714**, 365 (2004).
  - [21] J. M. Lattimer, C. J. Pethick, M. Prakash, and P. Haensel, *Phys. Rev. Lett.* **66**, 2701 (1991).
  - [22] D. Blaschke, H. Grigorian, and D. N. Voskresensky, *Astron. Astrophys.* **424**, 979 (2004).

- [23] S. Popov, H. Grigorian, R. Turolla, and D. Blaschke, *Astron. Astrophys.* **448**, 327 (2006).
- [24] T. Klähn, D. Blaschke, S. Typel, E. N. E. van Dalen, A. Faessler, C. Fuchs, T. Gaitanos, H. Grigorian, A. Ho, E. E. Kolomeitsev, et al., *Phys. Rev. C* **74**, 035802 (2006).
- [25] L. D. Miller and A. E. S. Green, *Phys. Rev. C* **5**, 241 (1972).
- [26] J. D. Walecka, *Ann. Phys. (N.Y.)* **83**, 491 (1974).
- [27] B. Serot and J. D. Walecka, *Adv. Nucl. Phys.* **16**, 1 (1986).
- [28] P. G. Reinhard, *Reports on Progress in Physics* **52**, 439 (1989).
- [29] P. Ring, *Prog. Part. Nucl. Phys.* **37**, 193 (1996).
- [30] B. D. Serot and J. D. Walecka, *Int. J. Mod. Phys. E* **6**, 515 (1997).
- [31] M. Bender, P.-H. Heenen, and P.-G. Reinhard, *Revs. Mod. Phys.* **75**, 121 (2003).
- [32] J. Meng, *Nucl. Phys. A* **635**, 3 (1998).
- [33] J. Meng and P. Ring, *Phys. Rev. Lett.* **77**, 3963 (1996).
- [34] J. Meng and P. Ring, *Phys. Rev. Lett.* **80**, 460 (1998).
- [35] J. Meng, I. Tanihata, and S. Yamaji, *Phys. Lett. B* **419**, 1 (1998).
- [36] J. Meng, H. Toki, S. G. Zhou, S. Q. Zhang, W. H. Long, and L. S. Geng, *Prog. Part. Nucl. Phys.* **57**, 470 (2006).
- [37] G. A. Lalazissis, J. König, and P. Ring, *Phys. Rev. C* **55**, 540 (1997).
- [38] S. Typel and H. H. Wolter, *Nucl. Phys. A* **656**, 331 (1999).
- [39] W. Long, J. Meng, N. Van Giai, and S.-G. Zhou, *Phys. Rev. C* **69**, 034319 (2004).
- [40] T. Nikšić, D. Vretenar, P. Finelli, and P. Ring, *Phys. Rev. C* **66**, 024306 (2002).
- [41] G. A. Lalazissis, T. Nikšić, D. Vretenar, and P. Ring, *Phys. Rev. C* **71**, 024312 (2005).
- [42] J. R. Oppenheimer and G. M. Volkoff, *Phys. Rev.* **55**, 374 (1939).
- [43] R. C. Tolman, *Phys. Rev.* **55**, 364 (1939).
- [44] N. K. Glendenning, *Compact Stars, Nuclear Physics, Particle Physics, and General Relativity* (Springer-Verlag, New York, 2000), 2nd ed.
- [45] R. Brockmann and H. Toki, *Phys. Rev. Lett.* **68**, 3408 (1992).
- [46] H. Lenske and C. Fuchs, *Phys. Lett. B* **345**, 355 (1995).
- [47] C. Fuchs, H. Lenske, and H. H. Wolter, *Phys. Rev. C* **52**, 3043 (1995).
- [48] J. Boguta and A. Bodmer, *Nucl. Phys. A* **292**, 413 (1977).
- [49] Y. Sugahara and H. Toki, *Nucl. Phys. A* **579**, 557 (1994).
- [50] B. D. Serot, *Phys. Lett. B* **86**, 146 (1979).
- [51] K. Sumiyoshi, H. Kuwabara, and H. Toki, *Nucl. Phys. A* **581**, 725 (1995).
- [52] F. Hofmann, C. M. Keil, and H. Lenske, *Phys. Rev. C* **64**, 025804 (2001).
- [53] S. F. Ban, J. Li, S. Q. Zhang, H. Y. Jia, J. P. Sang, and J. Meng, *Phys. Rev. C* **69**, 045805 (2004).
- [54] N. K. Glendenning, *Phys. Lett. B* **114**, 392 (1982).
- [55] N. K. Glendenning, *Astrophys. J.* **293**, 470 (1985).
- [56] R. Knorren, M. Prakash, and P. J. Ellis, *Phys. Rev. C* **52**, 3470 (1995).
- [57] J. Schaffner and I. N. Mishustin, *Phys. Rev. C* **53**, 1416 (1996).
- [58] C. J. Horowitz and J. Piekarewicz, *Phys. Rev. Lett.* **86**, 5647 (2001).

- [59] C. J. Horowitz and J. Piekarewicz, *Phys. Rev. C* **64**, 062802(R) (2001).
- [60] B. A. Brown, G. Shen, G. C. Hillhouse, J. Meng, and A. Trzcińska, *Phys. Rev. C* **76**, 034305 (2007).
- [61] C. J. Horowitz and J. Piekarewicz, *Phys. Rev. C* **66**, 055803 (2002).
- [62] H. Huber, F. Weber, and M. K. Weigel, *Phys. Rev.* **50**, R1287 (1994).
- [63] L. Engvik, M. Hjorth-Jensen, E. Osnes, G. Bao, and E. Østgaard, *Phys. Rev. Lett.* **73**, 2650 (1994).
- [64] P. G. Krastev and F. Sammarruca, *Phys. Rev. C* **74**, 025808 (2006).
- [65] M. Baldo, I. Bombaci, and G. F. Burgio, *Astron. Astrophys.* **328**, 274 (1997).
- [66] X. R. Zhou, G. F. Burgio, U. Lombardo, H.-J. Schulze, and W. Zuo, *Phys. Rev. C* **69**, 018801 (2004).
- [67] W. H. Long, N. V. Giai, and J. Meng, *Phys. Lett. B* **640**, 150 (2006).
- [68] W. H. Long, H. Sagawa, N. V. Giai, and J. Meng, *Phys. Rev. C* **76**, 034314 (2007).
- [69] W. H. Long, H. Sagawa, J. Meng, and N. V. Giai, *Europhysics Letters* **82**, 12001 (2008).
- [70] H. Liang, N. VanGiai, and J. Meng, *Phys. Rev. Lett.* **101**, 122502 (2008).
- [71] W. H. Long, H. Sagawa, J. Meng, and N. V. Giai, *Phys. Lett. B* **639**, 242 (2006).
- [72] A. Bouyssy, J. F. Mathiot, N. VanGiai, and S. Marcos, *Phys. Rev. C* **36**, 380 (1987).
- [73] G. Baym, C. J. Pethick, and P. Sutherland, *Astrophys. J.* **170**, 299 (1971).
- [74] G. Baym, H. A. Bethe, and C. J. Pethick, *Nucl. Phys. A* **175**, 225 (1971).
- [75] P. G. Reinhard, M. Rufa, J. Maruhn, W. Greiner, and J. Friedrich, *Z. Phys. A* **323**, 13 (1986).
- [76] M. M. Sharma, M. A. Nagarajan, and P. Ring, *Phys. Lett. B* **312**, 377 (1993).
- [77] I. Bombaci and U. Lombardo, *Phys. Rev. C* **44**, 1892 (1991).
- [78] L. Lindblom, *Astrophys. J.* **278**, 364 (1984).
- [79] N. K. Glendenning, *Phys. Rev. D* **46**, 4161 (1992).